Self-Assembled Nanostructured Materials

Janos H. Fendler

Department of Chemistry and the W. M. Keck Center for Molecular Electronics, Syracuse University, Syracuse, New York 13244-4100

Received February 9, 1996. Revised Manuscript Received May 17, 1996[⊗]

The "wet" colloid chemical construction of *nanosized* or *nanostructured materials* (i.e., those in the 1−100 nm range) has been inspired by *biomineralization* (the in vivo formation of inorganic crystals and/or amorphous particles in biological systems) and *hierarchically organized self-assembly* (spontaneous stepwise assembly of functional units). Subsequent to a summary of the molecular level organization of surfactant monolayers, Langmuir−Blodgett and self-assembled films emphasis is placed on the colloid chemistry underlying the self-assembly of nanostructured materials. Specifically, details are provided on (i) the preparation and stabilization of nanoparticle dispersions, (ii) the adsorption and desorption of nanoparticles onto solid surfaces, and (iii) the nanoreactors provided by polar liquids selectively adsorbed onto solid surfaces from binary polar−apolar liquid mixtures. The "wet" colloid chemical preparation of nanostructured materials in our laboratories is illustrated by the layer-by-layer self-assembly of (i) polyelectrolyte−semiconductor nanoparticle, (ii) polyelectrolyte−clay platelets−semiconductor nanoparticle, and (iii) polyelectrolyte−graphite oxide (and reduced graphite oxide) ultrathin films.

1. Introduction

1.1. Genesis of Wet Colloid Chemical Self-Assembly. *Nanosized* or *nanostructured materials* have dimensions, as their name implies, in the 1−100 nm range. It is at this size regime that many recent advances have been made in biology, physics, and chemistry. Nanostructured materials are synthesized in nature by a process known as biomineralization (the in vivo formation of inorganic crystals and/or amorphous particles in biological systems).[1−3] Biomineralization is believed to be mediated by proteins acting as templates at membrane interfaces. Most naturally occurring nanostructured materials are *hierarchically organized materials*.[4] This term implies an organization of materials in discrete steps, ranging from the atomic to the macroscopic scale, for optimal overall performance. The structure of abalone shell is a good illustration of a "bricks-and-mortal" hierarchial architecture. Calcium carbonate (aragonite) bricks are bonded by soluble acidic proteins and polysaccharides (i.e., the mortal) which are present in the abalone wall. This "bricks-and-mortal" construction imparts a great deal of structural strength to the shell while reducing cracking.

The physics of nanosized materials are described in terms of size quantization. Size quantization occurs at dimensions comparable to the length of the de Broglie electron, the wavelength of phonons, and the mean free path of excitons.[5−7] Electron−hole confinement in nanosized, spherical semiconductor particles results in three-dimensional size quantization, i.e., in the formation of "quantum dots", "quantum crystallites", or "zero-dimensional excitons". Two-dimensional confinement of the charge carriers results in "quantum well wires", "quantum wires", or "one-dimensional excitons" (i.e., the exciton is provided with only one-dimensional mobility). Finally, in one-dimensional size quantization, the exciton is permitted to move in two-dimensions ("two-dimensional excitons") with the resultant formation of "quantum wells". Bandgap engineering by size and dimension quantization is important since it leads to mechanical, chemical, and electrical, optical, magnetic, electrooptical, and magnetooptical properties that are substantially different from those observed for the bulk material.[5−7] For example, quantum dots can be tuned by changing their diameters to absorb and emit light at any desired wavelength. This property makes it feasible to construct a finely tunable and efficient semiconductor laser.[8] Semiconductor quantum dots can, in principle, be designed to capture a single electron at a time.[9,10] Exploitation of this concept will open the door for the manufacturing of ultrahigh-density integrated circuits and information storage devices which are based on the presence or absence of individual electrons.

Colloid chemists have traditionally dealt with dispersed particles, usually in the micrometer-to-submicrometer range. More recently their attention has focused upon nanometer regime. The construction of nanostructured materials by "wet" colloid chemical methods has been inspired by mother nature's organizational ability.[11] The term *self-assembly* implies the spontaneous adsorption of molecules or of nanoparticles, in a monoparticularly thick layer, onto a substrate. *Self-assembled multilayer films* are formed by the adsorption of subsequent monolayers of molecules or nanoparticles. The evolution of self-assembled layers of molecularly nanostructured materials can be traced, at least conceptually, from simple surfactant monolayers and multilayers, through their more complex particulate analogues to the self-assembly of simple molecules and larger particulates. Only an extremely brief outline of this evolution is provided in the present section. Available books and review articles on surfactant monolayers and multilayers, mono- and multiparticulate Langmuir−Blodgett (LB) films, self-assembled surfactants

[⊗] Abstract published in *Advance ACS Abstracts,* July 15, 1996.

S0897-4756(96)00116-0 CCC: $12.00

Table 1. Properties of Langmuir−Blodgett and Self-Assembled Films

	LB film	self-assembled film
film-forming materials	subphase insoluble (usually surface active) materials which can be compressed two-dimensionally	any charged material which has the appropriate adsorption−desorption properties
preparation method	monolayers, compressed in the film balance, are transferred by repeated substrate dipping and withdrawal (X-, Y-, or Z-type deposition)	(i) prepared substrate immersed in dispersion containing charged materials for a time optimized for adsorption, (ii) withdrawn substrate rinsed and washed, (iii) i and ii repeated for oppositely charged materials for the desired number of times
thickness, area	determined the thickness of the monolayer and the number of layers deposited (>300 layers reported), area is limited by the deposition equipment	determined the size (usually diameter) of the material and the number of layers deposited (50 layers reported), no deposition equipment is needed thus there are few practical limitation to area
forces	weak van der Waals interactions	strong ionic or coordinative bonds
order, stability	good layer-to-layer separation and two-dimensional order, pinholes and imperfections (decrease with thicker films), limited long-term mechanical stability in air, water, and some polar solvents	some intermingling of layers, pinholes and imperfections (decrease with thicker films), good long term mechanical stability in air, water and some polar solvents

and self-assembled polymers and particulate systems should be consulted for greater details.[12−14]

Molecular level organization of surfactants has been investigated for more than a century. Techniques for handling monolayers of surfactants were developed by Agnes Pockels in 1891,[15] and Irving Langmuir and Katherine Blodgett demonstrated, in the 1930s, that compressed monolayers of surfactants could be transferred, layer-by-layer, onto solid substrates to form ultrathin stable films, which are now referred to as Langmuir−Blodgett films.[16] It was Hans Kuhn and coworkers who showed, in the early 1970s, that LB films can have properties that are not exhibited by the individual monolayers.[17] In particular, these workers constructed energy-transfer systems, based on functionalized cyanine dyes, which mimicked the spectral sensitization of the photographic process.[18,19]

The recognition of the potential of molecularly organized films as advanced materials has fueled the renaissance of this area in the 1980s. An increasing number of research groups focused their attention to the construction, characterization, and potential utilization of monolayers and LB films. Fresh insights have been gained by multidisciplinary approaches and by employing new theories and experimental techniques.[13] These developments have led, in turn, to the construction of self-assembling monolayers (SAMs). SAMs obviate the need for surfactant compression in a Langmuir balance but require strong chemical interactions to anchor the appropriately functionalized surfactant to the well-cleaned substrate surface. The formation of a SAM was first reported by Sagiv, who immersed scrupulously clean substrates into a dilute solution of *n*-octadecyltrichlorosilane (OTS) in an organic solvent.[20] Self-assembly involved chemisorption of OTS and subsequent hydrolysis of the Si−Cl bonds at the substrate surface to form a Si−OSi network. Alternatively, thiol- and disulfide-functionalized surfactants have been self-assembled onto coinage metal surfaces, primarily by chemisorption.[21] Self-assembling of multilayers of surfactants was accomplished by sequential steps of (i) adsorbing thiol (or dithiol) surfactants, terminally functionalized either prior or subsequent to the adsorption, onto the coinage metal surfaces, (ii) chemically linking the second layer of functionalized surfactants to the anchored monolayer, and (iii) repeating step ii by the desired number of times. Self-assembly of complex superlattices have been recently reported.[22]

The construction of monolayers and self-assembled films has not been limited to surfactants. The methodology has been extended to larger molecules and, indeed to supramolecular assemblies. Thus, Langmuir films have been formed from fullerenes, polyelectrolytes, polystyrene microspheres, silylated glass beads, and surfactant-coated metallic, semiconductor, magnetic, and ferroelectric nanoparticles.[23] The self-assembly of supramolecular systems can be traced to the reported adsorption of negatively charged colloidal silica, or polystyrene latex particles, onto a cationic surfactant modified surface.[24] The adsorbed anionic colloidal particles have been shown, in turn, to adsorb a monoparticulate layer of positively charged colloids which, then adsorbed negatively charged colloidal particles from their dispersions. Repeated adsorptions, rinsing, and drying of negatively and positively charged colloidal particles resulted in the buildup of films, consisting of desired number of monoparticulate layers.[24] Subsequently, oppositely charged polyelectrolytes[25,26] and polyelectrolytes and clay platelets[27] have been self-assembled onto solid substrates.

1.2. LB and Self-Assembled Films Compared and Contrasted. It is instructive to compare and contrast nanostructured films prepared by the Langmuir−Blodgett technique and those formed by self-assembly. Although both methods yields molecularly (or supramolecularly) organized ultrathin films, the two-dimensional compression of monolayers (or monoparticulate films) on the water surface permit a better organizational control of the LB films than that obtainable for the spontaneously self-assembled films (see Table 1). Self-assembly is much more versatile, however. A greater variety of molecules and supramolecular assemblies can be self-assembled than compressed to stable monolayers. Furthermore, no special film balance is required for self-assembly; indeed the method has been referred to as a "molecular beaker epitaxy".[28] Appropriately selected oppositely charged materials are held together by strong ionic bonds and thus form long-lasting and stable self-assembled films which are often impervious to solvents. In contrast, LB films are less stable since they are maintained by weak van der Waals interactions. Some imperfections remain in both types of films. They are caused by impurities and by the presence of boundaries between the different domains of the substrate and of the film forming materials. Properties of LB and self-assembled films are sum-

marized in Table 1. Films can, of course, be prepared by alternating the LB technique with self-assembly for the deposition of any single layers materials at any desired order.[29]

1.3. Aims, Scopes, and Limitations. The understanding of colloid and surface chemistry is an essential requirement for the construction of self-assembled nanostructured materials. The primary aim of this review is, therefore, to survey the colloid and surface chemistry of stable monodisperse nanoparticles, their self-assembly onto solid substrates, and the properties of the liquid adsorption layer developed at the interface of the self-assembled nanoparticles in liquid mixtures. Details will be provided on the preparation and characterization of ultrathin films formed by the self-assembly of alternating layers of polyelectrolyte−semiconductor nanoparticles,[30] polyelectrolyte−exfoliated clay platelet−semiconductor nanoparticles,[30] and polyelectrolyte−graphite platelets.[31] Emphasis will be placed on results obtained in our own laboratories. Related self-assembly of nanostructured materials from inorganic solids, particularly zirconium phosphonates,[32] lipid tubules,[33] on solid substrates or on silicon,[34,35] or biosurfaces[36] as well as the use of self-assembled films for molecular recognition,[37] will not be discussed here.

The reader should be aware of the extensive and pertinent work published by researchers in marginally different disciplines. Thus, while electrodeposition cannot strictly be called self-assembly, many of the recent advances in constructing chemically modified electrodes[38] and depositing nanometer-scale layered structures by pulsing the applied potential during deposition[39] are clearly relevant to the present review. Similarly, chemists should keep in mind the spectacular accomplishments of solid-state bandgap engineering.

2. Colloid and Surface Chemistry of Self-Assembly

2.1. Preparation and Stability of Nanoparticle Dispersions. Developing reproducible preparations of stable dispersions containing monodispersed nanoparticles in desired compositions, sizes, and morphologies is the basic requirement for self-assembly. Equally important is the long-term stabilization of the nanoparticle dispersions.

Metallic, semiconducting, magnetic, and ferroelectric nanoparticles have been prepared by a large variety of different methods including hydrolysis and reduction of appropriate precursors, thermal decomposition, photolysis, and radiolysis.[14] New methods of preparation are being continuously discovered. This activity is fueled by the fundamental importance and potential applicability of nanostructured materials. Unfortunately, the mechanism of formation or monodisperse nanoparticles is not entirely understood. Careful attention to purity, to the concentrations of the reagents, to the rate and order of their addition, and to the temperature is the minimum requirement for the reproducible formation of nanoparticles in desired composition and size distribution.

van der Waals attraction between unprotected nanoparticles results in their coagulation and ultimate settling out of the particles from solution. Nanoparticle dispersions can be stabilized electrostatically and sterically.[40] The electrostatic stabilization involves the formation of an electrical double layer by the addition of counterions (citrate and chloride ions for gold and hexametaphosphate ion for sulfide semiconductor nanoparticles, for example). Agglomeration of the highly charged nanoparticles is prevented then by the screening of the Columbic repulsions which decays exponentially with increasing interparticle distances. Displacement of the adsorbed anions by a more strongly bound neutral molecule or cation will reintroduce the van der Waals attraction and thus it will result in coagulation.

Coating nanoparticles by polymers or surfactants sterically stabilizes them. Steric stabilization originates in entropic and osmotic effects. The entropy effect can be understood in terms of the required reorganization of the surfactant coating around the nanoparticles if they are to be packed tighter. Decreasing the distance between nanoparticles would force the stabilizing polymers or surfactants into a smaller and more restricted space—a process which would decrease the entropy of the system. Decrease of the entropy renders, of course, a closer approach of the nanoparticles to be thermodynamically unfavorable. The osmotic effect stabilizes the nanoparticles by increased solvation of the polymer chains which are present in higher concentration in the interparticle regions. Size-quantized nanoparticles have been recently stabilized by the covalent or coordinate addition of phosphine or thiol ligands.[41]

It should be mentioned that the monodispersity of nanoparticles have been substantially increased by gel filtration or size selected precipitation.[14]

2.2. Adsorption and Desorption of Nanoparticles onto Solid Surfaces. Self-assembly of nanoparticles to the oppositely charged substrate surface is governed by a delicate balance of the adsorption and desorption equilibria. The efficient adsorption of one (and only one) monoparticulate layer of nanoparticles onto the oppositely charged substrate surface is the objective of the immersion step. Preventing the desorption of the nanoparticles during the rinsing process is of equal importance. The optimization of the self-assembly in terms of maximizing the adsorption of nanoparticles from their dispersions and minimizing their desorption on rinsing requires the judicious selection of stabilizer(s) and the careful control of the kinetics of the process. The self-assembly of CdS and PbS nanoparticles was found to be most efficient, for example, if the semiconductor particles were coated by a 1:3 mixture of thiolactic acid and ethyl mercaptane.[30] It has to be admitted that this composition of the capping agent was arrived at by many trial and error experiments.

2.3. Nanoreactors Provided by Polar Liquids Selectively Adsorbed onto Solid Surfaces from Binary Polar−Apolar Liquid Mixtures. The structure and composition of porous solids profoundly influence the adsorption of liquids at their interfaces. Generally, the composition of the adsorption layer at a solid interface, x_1^s, is different than that would be expected based on the equilibrium distribution of a given two component liquid (x_1 and x_2) in the absence of any immersed or dispersed solid. Stating it differently, solids immersed or dispersed in multicomponent solvents mediate a solvent sorting in their immediate vicinity. Advantage can, therefore, be taken of the adsorption layer to provide a nanophase reactor within

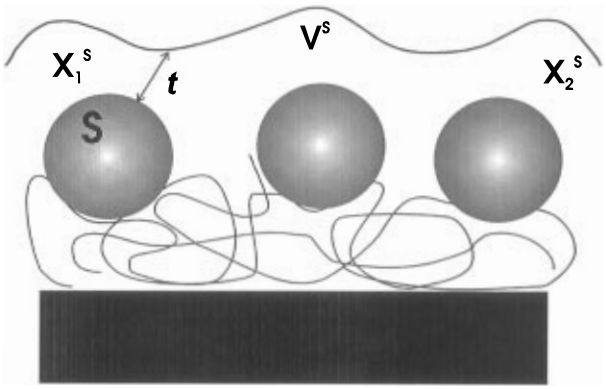

Figure 1. Schematics of the absorption layer, formed upon the immersion of a self-assembled nanoparticle film in a two-component (x_1 and x_2) liquid. S = solid phase of the nanoparticles, V^s = volume of the adsorption layer, t = thickness of the adsorption layer, and x_1^s = mole fraction of the component 1 present in the adsorption layer.

which size controlled particles can be in situ grown.

In binary mixtures the preferential adsorption of one of the two liquids (say, 1) in the interfacial adsorption layer is expressed by[42,43]

$$n_1^{\sigma(n)} = n^o(x_1^s - x_1)/m = n_1^s - (n_1^s + n_2^s)x_1 = n^s(x_1^s - x_1) \quad (1)$$

where $n_1^{(\sigma)n}$ is the adsorption excess amount of adsorbent (expressed as per m grams of adsorbent), n^o is the number of moles of the liquid mixture in the dispersed system, $n_1^s + n_2^s = n^s$ is the material content of the adsorption layer and $x_1^s = n_1^s/n^s$ (or $x_2^s = n_2^s/n^s$) is the composition of the adsorption layer (x_1 is the mole fraction of component 1). Preferential adsorption of one of the two liquids (say, 1) at the solid particle surface can occur to the extent that the adsorption layer practically consist of only component 1 (i.e., $x_1^s \gg x_2^s$ and $x_1^s \simeq 1$) even though the preferred liquid is only the minor component in the equilibrium mixture (i.e., $x_1 \ll 1$, $x_2 \simeq 1$, and $n_1^{\sigma(n)} \simeq n_1^s$).

The volume of the adsorption layer (V^s) can be calculated by the adsorption space filling model:[43]

$$V^s = a^s t = n_1^s V_{m,1} + n_2^s V_{m,2} + n_3 V_{m,3} + \ldots \quad (i = 1, 2, 3, \ldots) \quad (2)$$

where a^s is the available surface area (see Figure 1), t is the thickness of the adsorption layer, n_i^s is the amount of ith component, and $V_{m,i}$ is the molar volumes of the adsorbed ith component at the interface. If component 1 is adsorbed at the interface (i.e., $x_1^s \gg x_1$), then the volume of the adsorption layer can be expressed by

$$V^s = n_1^s V_{m,1} \quad (3)$$

Relatively simple adsorption excess isotherm measurements can be used for the determination of the values for the adsorption capacity (i.e., n_1^s, n_2^s, the material content of the adsorption layer), the adsorption volume (V^s) and the composition of the adsorption layer (x_1^s).

Generation of size-quantized semiconductor nanoparticles at dispersed organoclay complexes[43] and layered silicates[44] illustrate the use of the nanophase reactors provided by adsorbed binary liquids. The binary liquid pairs, ethanol(1)−cyclohexane(2) and methanol(1)−cyclohexane(2), were selected since the polar component of the liquid mixture (1) preferentially adsorbed at the solid interface hence its mole fraction in the bulk (x_1) was negligible (i.e., $x_1^s \gg x_1$ and $x_2^s \ll x_2$); and since the semiconductor precursors (Cd^{2+} and Zn^{2+}) were highly soluble in the liquid which preferentially adsorbed at the interface (methanol and ethanol) but was insoluble in the bulk phase (predominantly cyclohexane). These conditions effectively limited the nucleation and growth of the semiconductors to the nanophase reactor provided by the adsorption layer at the solid interface. By varying the mole fraction of the polar liquid (1) it was found possible to control the volume of the nanophase reactor and hence the size of the semiconductor particles grown therein. Extension of these principles to self-assembled films is the subject of our current research activities.[31]

3. Layer-by-Layer Self-Assembly of Polyelectrolyte−Inorganic Nanoparticle Sandwich Films

3.1. Alternating Layers of Polyelectrolyte−Semiconductor Nanoparticles. The layer-by-layer self-assembly of polyelectrolyte−semiconductor nanoparticles onto substrates is deceptively simple. A well-cleaned substrate is primed by adsorbing a layer of surfactant or polyelectrolyte onto its surface. The primed substrate is then immersed into a dilute aqueous solution of a cationic polyelectrolyte, for a time optimized for adsorption of a monolayer, rinsed, and dried. The next step is the immersion of the polyelectrolyte monolayer covered substrate into a dilute dispersion of surfactant-coated negatively charged semiconductor nanoparticles, also for a time optimized for adsorption of a monoparticulate layer, rinsing, and drying. These operations complete the self-assembly of a polyelectrolyte monolayer−monoparticulate layer of semiconductor nanoparticle sandwich onto the primed substrate. Subsequent sandwich units are deposited analogously. The method is illustrated by the self-assembly of a poly(diallylmethylammonium chloride), P, CdS nanoparticle film onto different substrates, S (gold, silver, platinum, quartz slide, highly ordered pyrolytic graphite, HOPG, mica, and Teflon).[30] The procedure involved the following steps: (i) immersion of the well cleaned (soaked in a concentrated sulfuric acid solution of Nocromix for 0.5−3 hours, repeatedly rinsed by ample amounts of deionized water, and dried) S into a 1.0%, w/v, aqueous solution of P, kept at pH = 8.5 (no buffer), for 15 min; (ii) rinsing with a stream of deionized distilled water, kept at pH = 8.5; (iii) immersion into an aqueous CdS nanoparticle dispersion, kept at pH = 9−10, for 24 h; and (iv) washing with a stream of deionized water, kept at pH = 8.5. Each washing was followed with drying by a stream of N_2 for 30 s. Thus, performing steps i−iv led to the self-assembly of a one layer of polycation−one layer of CdS nanoparticle sandwich unit on the substrate, for which we adopted the S−(P/CdS) shorthand notation. Subsequent P−CdS nanoparticle sandwich units were self-assembled by repeating steps i−v n times to produce films comprised of n number of sandwich units, $S-(P/CdS)_n$ (see Figure 2 for self-assembly of an $S-(P/CdS)_n$ film). Similar methodologies (steps i−iv) were employed for the self-assembly of many

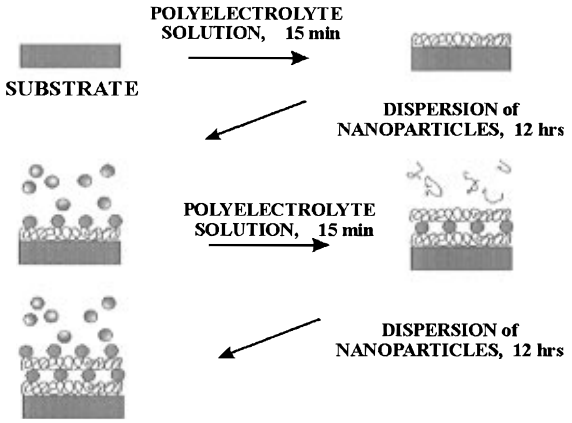

Figure 2. Schematics of the self-assembly of an S−(P/CdS)$_n$ film.

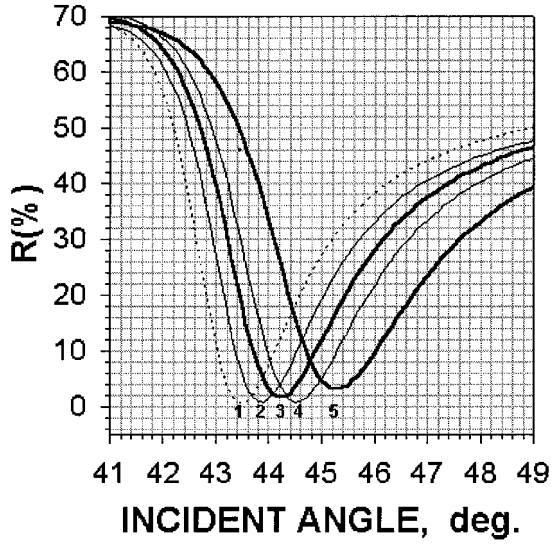

Figure 3. Surface plasmon spectroscopic curves for the sequential deposition of self-assembled layers: 1 = bare Au film, 2 = P on gold D_{Pl} = 18 Å, 3 = P/GO on gold D_{Gr} = 25 Å, 4 = (P/GO)P on gold D_{Pl} = 16 Å, 5 = (P/GO)$_2$ on gold D_{Gr} = 20 Å, 5 = (P/GO)$_2$P on gold D_{Pl} = 14 Å. Fitting parameters: $\epsilon_{polymer}$ = 2.25, ϵ_{GO} = 2.24 for all layers.

other polyelectrolyte−semiconductor nanoparticle sandwich films.

Absorption and emission spectrophotometry, surface plasmon spectroscopy, X-ray diffractometry, scanning force microscopy, and transmission electron microscopy have been used for monitoring the self-assembly and characterizing the structures of self-assembled films.[30]

Optimization of the self-assembly of the initial layer of P is of particular importance. The thickness of the initial layer of P, self-assembled on a gold electrode, was found to be dependent on the concentration of the polyelectrolyte and on the immersion time. This is illustrated by the surface plasmon spectroscopy of a series of depositions in different concentrations of P (Figure 3). Furthermore, soaking in an aqueous solution for 4 h did not remove P, as evidenced by the unaltered surface plasmon spectrum. AFM images of the polyelectrolyte film revealed featureless wavelike structures with height variations of about 0.2 nm (Figure 4). Apparently, multiple van der Waals forces maintain P on a variety of substrate surfaces, even in the absence of covalent bonding. Assuming P to be completely stretched on the surface of S, the mean area occupied by a positive charge on P can be estimated to be 10 Å^2. It is this surface charge and relatively high charge density which provide the electrostatic driving force for the self-assembly of the negatively charged, surfactant-stabilized CdS, PbS, and TiO_2 nanoparticles onto the positive surface of P. The absorption spectra of the semiconductor nanoparticle dispersions in aqueous solutions are retained in the self-assembled films (see Figure 5 for the spectra of CdS nanoparticles in their dispersions and in the self-assembled S−(P/CdS)$_{20}$ film). Furthermore, the absorption edges (ca. 430 nm for CdS and ca. 500 nm for PbS) correspond to mean particle diameters of 35 and 100 Å.

The AFM images of self-assembled CdS particles revealed the formation of a well-packed monoparticle layer (Figure 6). The successful self-assembly of a large number of repeating sandwich units of S−(P/CdS)$_n$, S−(P/PbS)$_n$, and S−(P/TiO_2)$_n$ was monitored by absorption and emission spectroscopic measurements. For example, the observed good linearities in the plots of absorbances vs n in S−(P/CdS)$_n$ and S−(P/PbS)$_n$ indicate the uniformity of the sandwich units that were self-assembled (see insert in Figure 5). Activated CdS nanoparticle dispersions showed a strong fluorescence with an emission maximum at 490 nm, which was attributed to the $1s_e-1s_h$ exitonic transition. Very similar emission spectra were obtained for the self-assembled S−(P/CdS)$_{20}$ films (Figure 6). Furthermore, the relative intensity of the emission was found to increase linearly with increasing P/CdS units, self-assembled on the substrate, up to n = 15 (see insert in Figure 6). The good linearity of the fluorescence intensity vs n plot indicates the uniformity of the self-assembled film. This was also confirmed by X-ray diffraction of a S−(P/CdS)$_{20}$ sample. The observed 2θ = 1.70 peak (not shown) corresponds to a 6.5 ± 0.8 nm repeating unit in the (P/CdS)$_{20}$ film. Since the CdS particle diameters were determined to be 4.0 ± 0.5 nm by dynamic light scattering, the difference (6.5 ± 0.8 nm − 4.0 ± 0.5 nm = 2.5 ± 0.5 nm) agrees well with that determined for the thickness of a polyelectrolyte layer by surface plasmon spectroscopy (2.0 ± 0.5 nm, vide supra).

3.2. Alternating Layers of Polyelectrolyte−Clay Platelets−Semiconductor−Nanoparticles. Smectic clays, such as Na^+−montmorillonite, have been exfoliated into (10 ± 2)-Å-thick layered silicates, often referred to as clay organocomplexes, by ion-exchange reaction with cationic surfactants.[30,31] The high lateral bond strength and aspect ratios have rendered clay organocomplexes to be eminently suitable materials for nanoconstruction. Indeed, the nanocomposites prepared by mixing polymers and clay organocomplexes had superior mechanical properties.[45] However, a layer-by-layer assembly of nanocomposites is required for the preparation of ultrathin films for advanced optical and electrooptical device construction. This has prompted the spreading of clay organocomplexes on water surfaces and their subsequent transfer to substrates by the Langmuir−Blodgett technique as well as the self-assembly of polyelectrolyte−clay platelet films.[46]

Alternating layers of polyelectrolyte (P)−clay platelet (M) sandwich films have self-assembled in a manner analogous to that shown for S−(P/CdS)$_n$ (Figure 2).[30] Significantly, the thickness of a given multilayer S−(P/

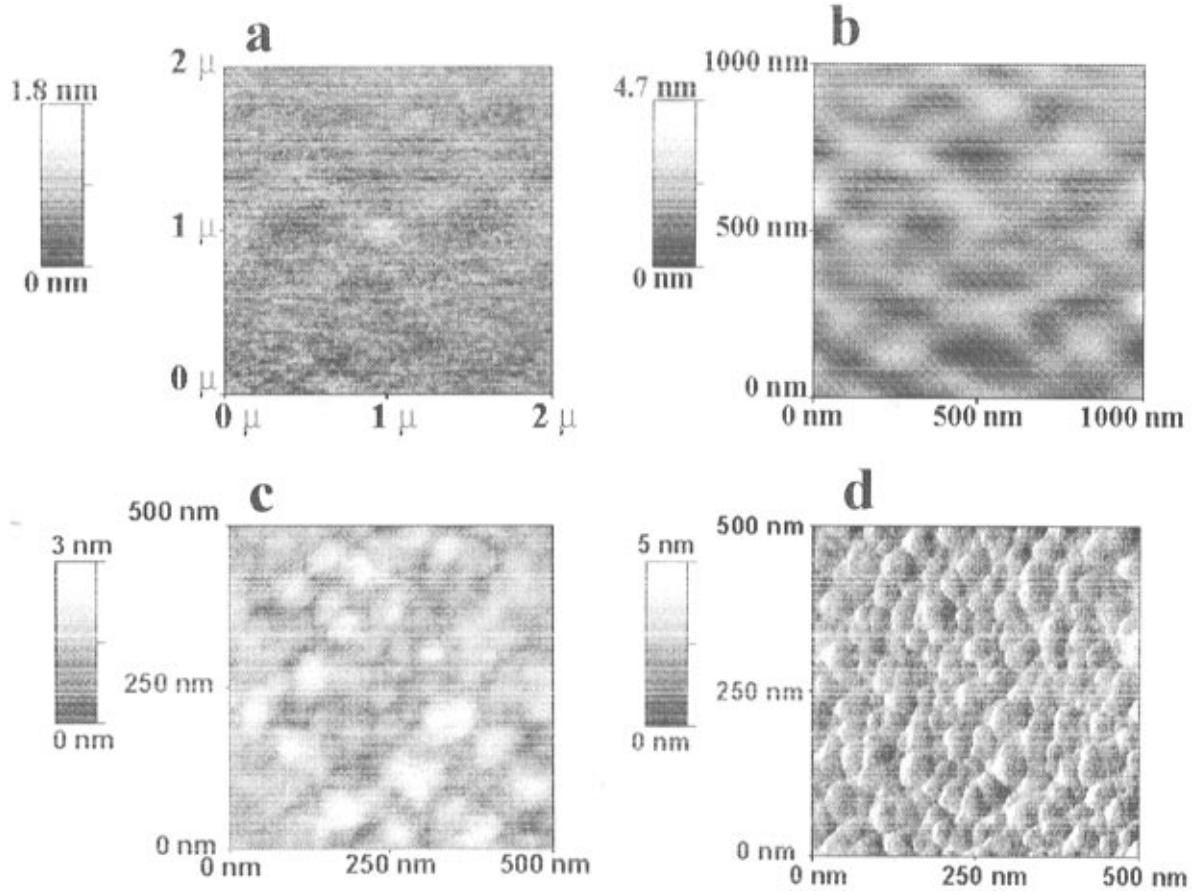

Figure 4. AFM images of a layer P (a), P/PbS (b), P/CdS (c), and P/TiO_2 (d) on mica.

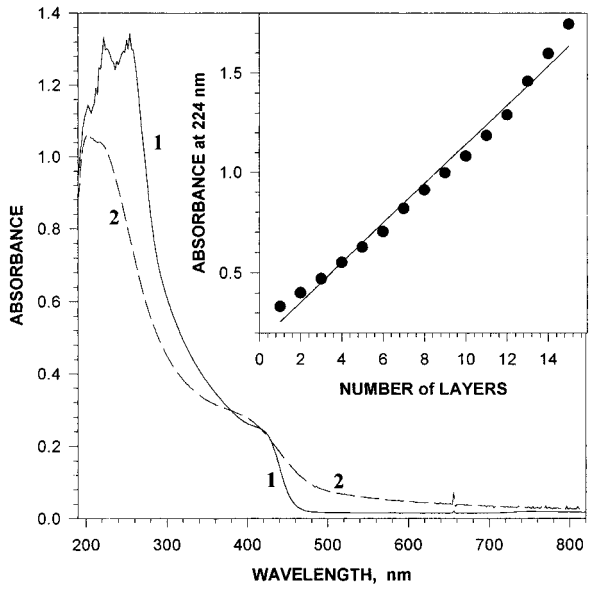

Figure 5. Absorption spectra of CdS nanoparticles in their dispersions (1) and in the self-assembled S−(P/CdS)$_{20}$ film. Insert shows a plot of absorbances at 244 nm vs the number of P\CdS sandwich unit self-assembled.

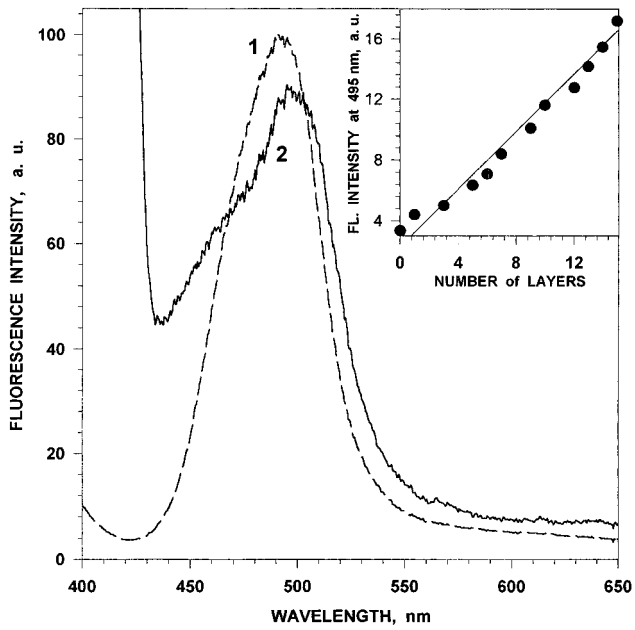

Figure 6. Emission spectra of CdS in their dispersions (1) and in the self-assembled S−(P/CdS)$_{20}$ film. Insert shows a plot of emission at 495 nm vs the number of P\CdS sandwich unit self-assembled.

M)$_n$ film was found to depend on the potential which was applied during the deposition(s) of M. This behavior was established by electrochemical and surface plasmon spectroscopic measurements. In the electrochemical measurements the working electrode was prepared by the sequential self-assembly of the required number (n) of (P/M) sandwich units on a platinum substrate (S). AgCl was used as the reference electrode. Cyclic voltammograms of 10 mM $K_3Fe(CN)_6$ in aqueous solutions provided useful information on the properties of the S(P/M)$_n$ film self-assembled onto the working electrode. Oxidations and reductions occurred at the metal electrode interface as a result of the diffusion-controlled penetration of the $Fe(CN)_6^{3-}$ and $Fe(CN)_6^{4-}$ ions through the self-assembled film. Increasing current drops upon the deposition of successive layers of

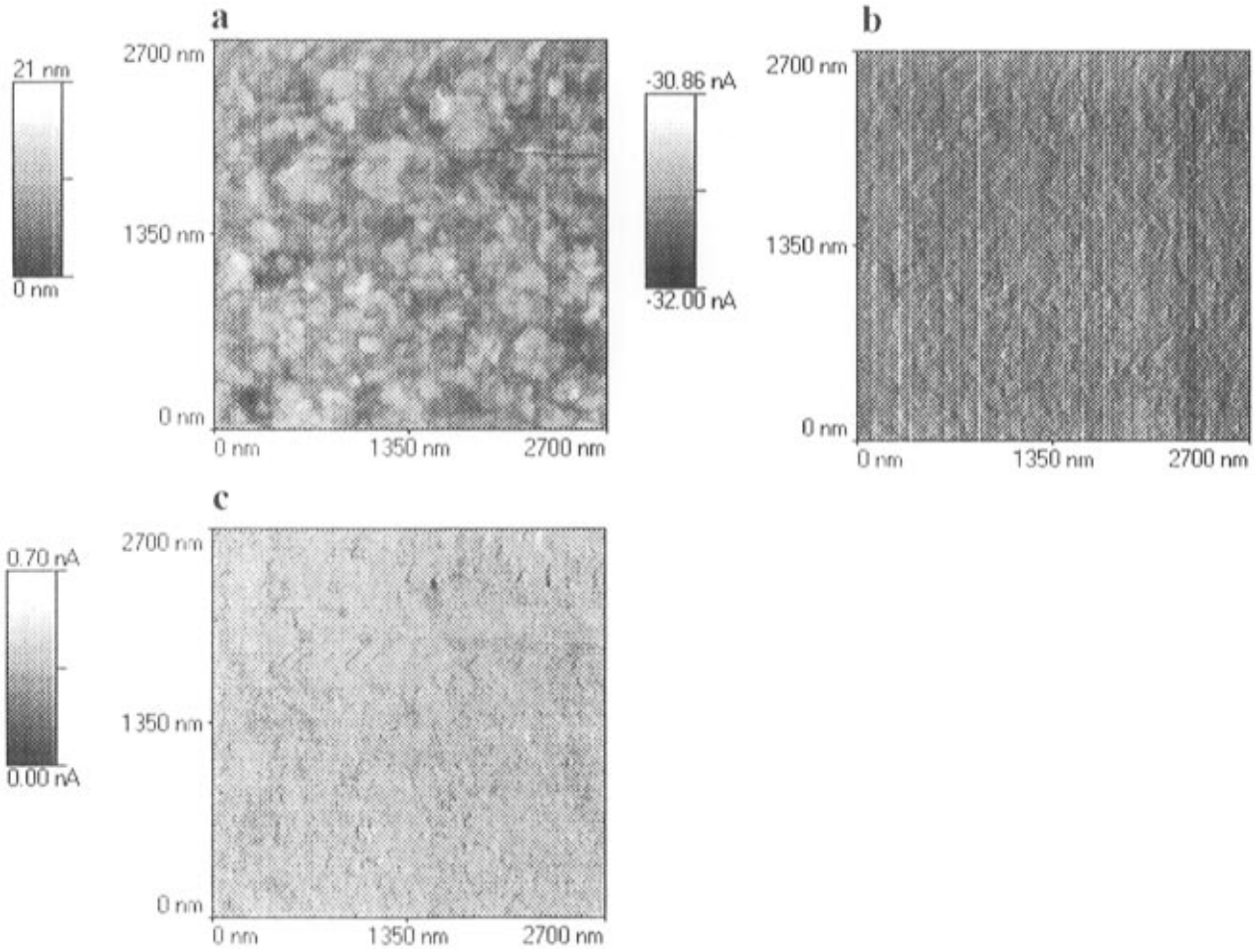

Figure 7. AFM images of one layer of M self-assembled on mica. a = topography, b = internal sensor, and c = lateral forces. Set point = −10 nA, scan rate = 200 nm/s, resolution = 200 lines.

P/M are clearly seen in the cyclic voltammograms. The thickness of a given multilayer film was found to depend on the potential which was applied during the deposition(s) of M. Positive potentials increased the film thickness, while negative ones decreased it. Not unexpectedly, negatively charged M is attracted to a positively charged electrode more efficiently than it is to a negatively charged one. Similar behavior has been noted in the electrophoretic deposition of metal particles onto conductive substrates.[30,31]

The effect of an applied potential during the self-assembly also manifested itself in the changes of the surface plasmon spectra of the self-assembled films. Self-assembly of M was also observed by using the topography, internal sensor, and lateral force modes of the AFM (Figure 7). The lateral force mode was found to be least informative due to the small height variation along the surface. The height variations did not exceed 5 nm in a 2700 nm interval as seen in the topographic images (see Figure 8a). The primary source of this height variation is the stacking of the clay platelets and adsorption of not-fully-exfoliated aggregates. Otherwise, the film is rather uniform and the planar orientation of the platelets is readily observable. The planar orientation of the montmorillonite platelets in self-assembled films is substantiated by their transmission electron micrograms (Figure 8).

X-ray diffraction measurements showed sharp peaks for $S-(P/M)_{20}$ at $2\theta = 2.1°$ which corresponded to planar periodicities of 4.3 ± 0.5 nm for the P/M repeating units.

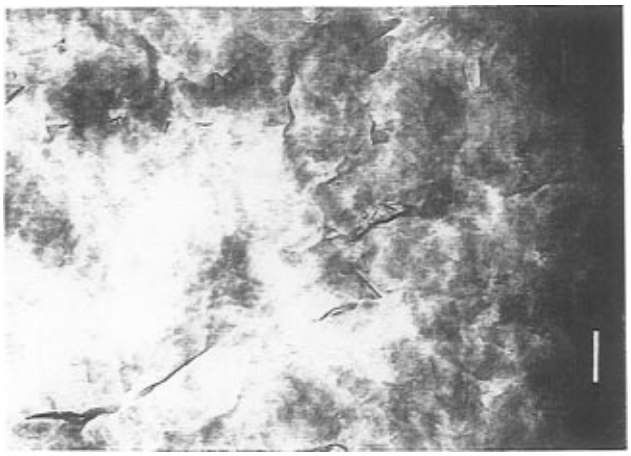

Figure 8. Transmission electron micrographs of one layer of M self-assembled onto one layer of polycation-coated substrate. The scale bar is 200 nm.

Since the thickness of the polyelectrolyte layer was determined by surface plasmon spectroscopy to be 2.0 ± 0.5 nm, each self-absorbed M must contain at least two layers of clay platelets (each with a thickness of 1.0 ± 0.1 nm). The second broad peak in the X-ray diffraction of $S-(P/M)_{20}$ films corresponds to the basal spacing between the clay platelets within one layer.

Versatility is the major advantage of the self-assembly described here. The method allows the construction of composite films comprising different nanoparticles which can be layered in any desired order. Indeed the self-

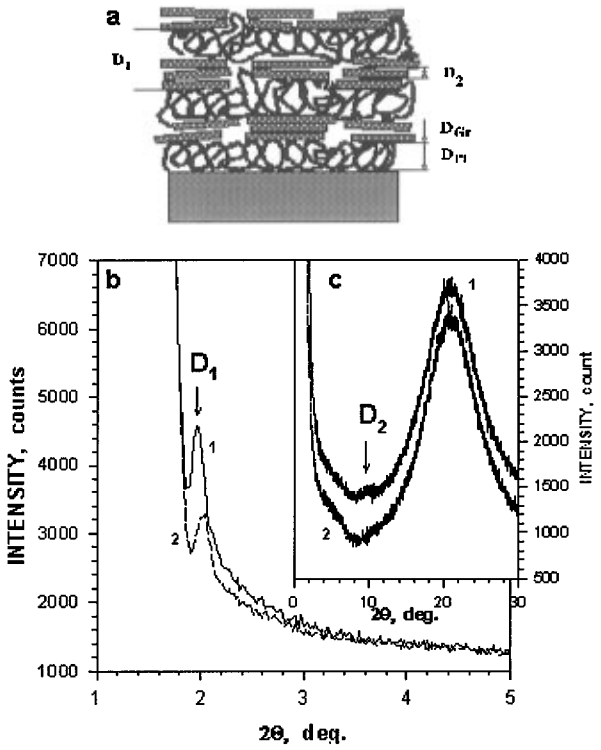

Figure 9. X-ray diffraction patterns and schematics of S−(P/GO)$_{30}$. D_1 = repeating P\GO units, D_2 = basal spacing, d_1 and d_2 distances determined by surface plasmon spectroscopy.

assembly of a variety of P/M/semiconductor nanoparticles have been reported.[30,31]

3.3. Alternating Layers of Polyelectrolyte−Graphite Platelets. Graphite (G), like silicates, has a highly ordered layered structure. Furthermore, ultrathin G/P composites have many potentially beneficial properties, including controllable conductivity and magnetoresistance.[47] Since G cannot be dispersed in water, a viable approach to form ultrathin S−(P/G)$_n$ films is to prepare exfoliated graphite oxide (GO) platelets, self-assemble them onto P covered (S), and then in situ reduce the S−(P/GO)$_n$ films. This approach has, in fact, been realized in our laboratories.[31]

The construction of a P/GO self-assembled sandwich unit involved the following steps: (i) immersion of S into a 2.0% (w/v) aqueous P solution, kept at pH = 8.5 (no buffer), for 15 min, (ii) rinsing with a stream of deionized distilled water, (iii) immersion into the aqueous GO dispersion, for 15 min, and (iv) washing with a stream of deionized water. Each washing was followed with drying by a stream of N_2 for 30 s. Thus, performing steps i−iv led to the self-assembly of a one layer of polycation−one layer of graphite oxide platelet sandwich unit on the substrate, S−(P/GO).[31] Subsequent P/GO sandwich units were self-assembled by repeating steps i−v n times to produce films comprised of n number of sandwich units, S−(P/GO)$_n$.

Self-assembly of the successive P/GO layers onto a quartz slide was monitored by absorption spectrophotometry. The thickness of one sandwich unit of P/GO was determined to be 3.8 ± 0.7 nm by surface plasmon spectroscopy.

X-ray diffraction spectra of S−(P/GO)$_{30}$ is illustrated in Figure 9. The basal spacing of 0.93 ± 0.05 nm agrees well with the value determined for a layer of graphite by surface plasmon spectroscopy.

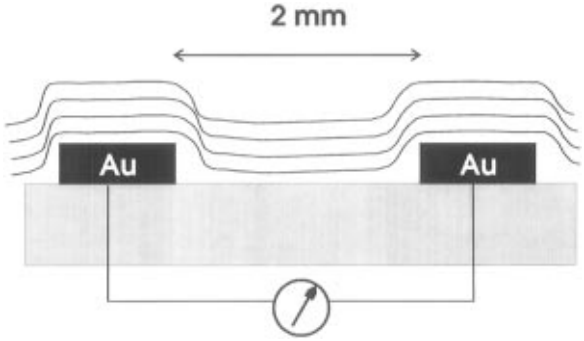

Figure 10. Schematics of the arrangements used for resistivity measurements.

Reduction of GO in the S−(P/GO)$_n$ films to graphite, G was accomplished either chemically or electrochemically. The chemical reduction involved the immersion of the self-assembled film into an aqueous hydrazine hydride (50%, w/v) solution for 1−24 h or into a 0.10 M HCl solution which contained Zn pellets (i.e., into a *nascent* hydrogen generator) for 2−3 h. The electrochemical reduction of GO (in the S−(P/GO)$_n$ film, self-assembled on metal or glassy carbon electrodes) was performed by scanning the potential from −0.5 to −1.5 V vs SCE for 20 min.

The extent of GO reduction was monitored by X-ray diffraction measurements and by absorption spectrophotometry. The reduction of GO to G was accompanied by a slight diminishing of the interlayer spacing (from 45.2 to 43.7 Å for the hydrazine reduction and from 56 to 45 Å for the electrochemical reduction. The small peak at 9.04 Å (corresponding to the interplatelet basal spacing) does not appear in the X-ray diffraction pattern of the reduced GO. However in reduced GO there is a shoulder at 5.7° (15.5 Å) corresponding to the basal spacing between the reduced GO platelets.

Cyclic voltammetry of an S−(P/GO)$_{16}$ film, self-assembled on metal or glassy carbon electrodes, revealed a peak positioned at −0.95 ± 0.05 V which correspond to the reduction of GO. This process is completely irreversible as evidenced by the absence of a peak on the reverse scan. Moreover this peak can only be observed in the first CV scan. After that the peak disappears indicating the complete reduction of GO. The dependence of the peak height vs the number of GO/P layers is linear up to the self-assembly of 8−10 sandwich units.

The lateral resistivity of a (P/GO)$_{10}$ film was measured between two 3 mm wide gold stripes evaporated on a glass slide at a distance of 2 mm between them (Figure 10). Self-assembled graphite oxide films were deposited on top of them over the whole surface of the slide. The as-deposited (P/GO)$_{10}$ film had an R value of 32 MΩ at the 2 mm gap. After reduction by hydrogen, evolving in situ, the R value dropped to 12 KΩ, which amounts to a 27 000-fold decrease in the overall resistance. This corresponds to the change in volume conductivity from $1.2 \times 10^4\ \Omega^{-1}\ m^{-1}$ to $3.1 \times 10^7\ \Omega^{-1}\ m^{-1}$. Roughening the substrate surface (by multiple diamond knife grooves along the electrode direction) *prior to* the deposition of multilayers rendered the resistivity decrease (which accompanied GO reduction) to be less pronounced (only a 370-fold increase in conductivity was observed). This was the consequence of imperfect self-assembly on a disturbed surface which resulted in broken films and

less than uniform in-plane contacts of the GO platelets.

Self-assembled composite (P/GO) films were found to be remarkably stable in concentrated acid or basic solutions and resisted photodegradation. The demonstrated lateral conductivities and the relative ease of transition between nonconductive GO state to conductive G state render these films inherently interesting and potentially useful as components of advanced optical and electronic devices.

4. Potential Applications

The relative ease of preparation and the high degree of versatility render self-assembled ultrathin films amenable to a large variety of diverse applications. Self-assembled films can function as membranes (barriers), with controllable levels of permeability, for gases, liquids, covalent molecules, ions, and, indeed, electrons (tunneling barriers). These properties have been exploited for the construction of insulators, passivators, sensors, and modified electrodes. Self-assembled nanostructured films are eminently suitable for the construction of devices based on molecular recognition. Molecules or supramolecular assemblies (nanoparticles) within a self-assembled layer can be aligned spontaneously, or by changing the temperature, pressure, and pH, or, alternatively and additionally, by the application of an electric or magnetic field. These characteristics permit the formation of superlattices with desired symmetry (or dissymmetry) and, hence, the fabrication of a host of photonic, electronic, magnetic, and nonlinear optical devices. The layer-by-layer self-assembly of insulators (appropriate hydrocarbon surfactants, for example), conductors (metallic nanoparticles, graphite, conducting polymers, for example), magnetic, ferroelectric, and semiconductors nanoparticulate films, in any desired order, allows the construction of molecularly (or supramolecularly) resolved heterostructures. These, in turn, afford the optimization of charge separation and carrier transport to the level necessary for the bandgap engineering of quantum devices. Control of the sizes and interparticle distances of the monodispersed nanoparticles within the self-assembled film can be exploited for such optical applications as the construction of Bragg diffraction devices for Raman spectrometers and for enhancing the Raman intensity by surface plasmon interactions.[48] Other applications are likely to be developed.

The outlook of self-assembled nanostructured materials is bright. We have applied only a small part of our chemical know-how to these inherently fascinating and highly rewarding field of investigations. I am confident that the next few years will witness an explosive growth of chemical research focused upon self-assembled nanostructured materials.

Acknowledgment. Support of this work by the National Science Foundation (U.S.A.) is gratefully acknowledged. True credit is due, of course, to my coworkers (whose names appear in the cited joint primary publications) for creative, dedicated, and skillful work.

References

(1) Mann, S. *Nature* **1993**, *365*, 499.
(2) Addadi, L.; Weiner, S. *Angew. Chem., Int. Ed. Engl.* **1992**, *31*, 153.
(3) Heywood, B. R.; Mann, S. *Adv. Mater.* **1994**, *6*, 9.
(4) Liu, J.; Sarikaya, M.; Aksay, I. A. *Mater. Res. Soc. Symp. Proc.* **1992**, *255*, 9.
(5) Colvin, V. L.; Goldstein, A. N.; Alivisatos, A. P. *J. Am. Chem. Soc.* **1992**, *114*, 5221.
(6) Henglein, A. *Ber. Bunsen-Ges. Phys. Chem. Chem. Phys.* **1995**, *99*, 903.
(7) Hodes, G. *Sol. Energy Mater. Sol. Cells* **1994**, *32*, 323.
(8) Colvin, V. L.; Schlamp, M. C.; Alivisatos, A. P. *Nature* **1994**, *370*, 354.
(9) Devoret, M. H.; Esteve, D.; Urbina, C. *Nature* **1992**, *360*, 547.
(10) Nakazato, K.; Ahmed, H. *Adv. Mater.* **1993**, *5*, 668.
(11) Mann, S. *Biomimetic Materials Chemistry*; VCH: New York, 1996.
(12) Fendler, J. H. *Membrane Mimetic Chemistry, Characterizations and Applications of Micelles, Microemulsions, Monolayers, Bilayers, Vesicles, Host-Guest Systems and Polyions*; John Wiley: New York, 1982.
(13) Fendler, J. H. *Membrane Mimetic Approach to Advanced Materials*; Springer-Verlag: Berlin, 1992.
(14) Fendler, J. H.; Meldrum, F. C. *Adv. Mater.* **1995**, *7*, 607.
(15) Pockels, A. *Nature* **1891**, *43*, 437.
(16) Blodgett, K. *J. Am. Chem. Soc.* **1934**, *56*, 495.
(17) Kuhn, V. H.; Möbius, D. *Angew. Chem., Int. Ed. Engl.* **1983**, *83*, 672.
(18) Möbius, D. *Acc. Chem. Res.* **1981**, *14*, 63.
(19) Kuhn, H.; Möbius, D. *Angew. Chem., Int. Ed. Engl.* **1971**, *10*, 620.
(20) Sagiv, J. *J. Am. Chem. Soc.* **1980**, *102*, 92.
(21) Nuzzo, R. G.; Allara, D. L.; Nuzzo, R. G.; Allara, D. L. *J. Am. Chem. Soc.* **1983**, *105*, 4481.
(22) Maoz, R.; Yam, R.; Berkovic, G.; Sagiv, J. In: *Organic Thin Films and Surfaces*; Ulman, A. Ed.; Academic Press: Cambridge, MA, 1995; Vol. 20, p 41.
(23) Meldrum, F. C.; Fendler, J. H. In *Biomimetic Materials Chemistry*; Mann, S., Ed.; VCH: New York, 1996; p 175.
(24) Iler, K. *J. Colloid Interface Sci.* **1966**, *21*, 569.
(25) Decher, G.; Sohling, U. *Ber. Bunsen-Ges. Phys. Chem.* **1991**, *95*, 1538. Decher, G.; Lvov, Y.; Schmitt, J. *Thin Solid Films* **1994**, *244*, 772.
(26) Cheung, J. H.; Punkka, E.; Rikukawa, M.; Rosner, R. B.; Royappa, A. T.; Rubner, J. F. *Thin Solid Films* **1992**, *210/211*, 246.
(27) Kleinfeld, E. R.; Ferguson, G. S. *Science* **1994**, *265*, 370.
(28) Keller, S. W.; Kim, H. N.; Mallouk, T. E. *J. Am. Chem. Soc.* **1994**, *116*, 8817.
(29) Ulman, A. *An Introduction to Ultrathin Organic Films, From Langmuir-Blodgett to Self-Assembly*; Academic Press: Boston, 1991.
(30) Kotov, N. A.; Dékány, I.; Fendler, J. H. *J. Phys. Chem.* **1995**, *99*, 13065.
(31) Kotov, N. A.; Dékány, I.; Fendler, J. H. *Adv. Mater.*, in press.
(32) Keller, S. W.; Johnson, S. A.; Brigham, E. S.; Yonemoto, E. H.; Mallouk, T. E. *J. Am. Chem. Soc.* **1995**, *117*, 12879.
(33) Schnur, J. M.; Shashidhar, R. *Adv. Mater.* **1994**, *6*, 971.
(34) Vaia, R. A.; Vasudevan, S.; Krawiec, W.; Scanlon, L. G.; Giannelis, E. P. *Adv. Mater.* **1995**, *7*, 154.
(35) Schilling, M. L.; Katz, H. E.; Stein, S. M.; Shane, S. F.; Wilson, W. L.; Buratto, S.; Ungashe, S. B.; Taylor, G. N.; Putvinski, T. M.; Chidsey, C. E. D. *Langmuir* **1993**, *9*, 2156.
(36) Kumar, A.; Abbott, N. L.; Kim, E.; Biebuyck, H. A.; Whitesides, G. M. *Acc. Chem. Res.* **1995**, *28*, 219.
(37) Freeman, R. G.; Grabar, K. C.; Allison, K. J.; Bright, R. M.; Davis, J. A.; Guthrie, A. P.; Hommer, M. B.; Jackson, M. A.; Smith, P. C.; Walter, D. G.; Natan, M. J. *Science* **1995**, *267*, 1629.
(38) Bard, A. J.; Mallouk, T. In *Molecular design of electrode surfaces*; Vol. XXII., Murray, R. W., Ed.; John Wiley & Sons: New York, 1992; p 270.
(39) Switzer, J. A.; Shane, M. J.; Phillips, R. J. *Science* **1990**, *247*, 444. Yoneyama, H. *Adv. Mater.* **1993**, *5*, 394. Switzer, J. A.; Hung, C. J.; Breyfogle, B. E.; Shumsky, M. G.; Vanleeuwen, R.; Golden, T. D. *Science* **1994**, *264*, 1573.
(40) Adamson, A. *Physical Chemistry of Surfaces*, 5th ed.; John Wiley: New York, 1990.
(41) Alivisatos, A. P. *Mater. Res. Soc. Bull.* **1995**, *20*, 23.
(42) Dékány, I.; Nagy, L. G. *Colloids Surf.* **1991**, *58*, 251.
(43) Dékány, I.; Turi, L.; Tombácz, E.; Fendler, J. H. *Langmuir* **1995**, *11*, 2285.
(44) Dékány, I.; Nagy, L.; Turi, L.; Király, Z.; Kotov, N. A.; Fendler, J. H., unpublished work, 1996.
(45) Lan, T.; Pinnavaia, T. J. *Chem. Mater.* **1994**, *6*, 2216.
(46) Kotov, N. A.; Meldrum, F. C.; Fendler, J. H.; Tombacz, E.; Dekany, I. *Langmuir* **1994**, *10*, 3797.
(47) Ponomarenko, A. T.; Shevchenko, V. G.; Klason, C.; Pristupa, A. I. *Smart Mater. Struct.* **1994**, *3*, 409.
(48) Asher, S. A.; Holtz, J.; Liu, L.; Wu, Z. *J. Am. Chem. Soc.* **1994**, *116*, 4997.

CM960116N